© 2022 IEEE. Personal use of this material is permitted. Permission from IEEE must be obtained for all other uses, in any current or future media, including reprinting/republishing this material for advertising or promotional purposes, creating new collective works, for resale or redistribution to servers or lists, or reuse of any copyrighted component of this work in other works.

Direct Bandgap Control by Narrowing the Germanium Strip Structure on Silicon for C+L Band Photonic Devices

Shuhei Sonoi, Riku Katamawari, Manami Shimokawa, Kyosuke Inaba, Jose A. Piedra-Lorenzana, Takeshi Hizawa, Junichi Fujikata, and Yasuhiko Ishikawa, *Member, IEEE*

***Abstract*—This study reports the bandgap engineering of a Ge epitaxial layer on Si to tune the operating wavelength of optical intensity modulators and photodetectors in the C (1.530–1.565 µm)+L (1.565–1.625 µm) band. A strip structure of elemental Ge is investigated, rather than wider-gap SiGe or narrower-gap GeSn alloy, to achieve the key property of a C band modulation and improved L band detection. By narrowing the strip to the submicron scale, a tensile lattice strain in Ge, induced by a thermal expansion mismatch with Si, is elastically relaxed by an edge-induced relaxation effect. The photoluminescence peak and photodetection spectra show a significant blue shift as the narrowed direct gap of ~0.77 eV is restored to 0.80 eV of unstrained Ge. A standard SiN_x external stressor on a narrow Ge strip induces an increased blue shift or an opposite red shift, depending on the stress polarity in SiN_x. The results show that it is possible to tune the operating wavelength of modulators and photodetectors of elemental Ge in the C+L band.**

***Index Terms*—Band engineering, germanium, intensity modulation, photodetectors, silicon photonics**

I. Introduction

Ge is the standard material for a near-infrared photodetector (PD) in Si photonics [1–25]. The Ge thickness is typically several 100 nm in a PD integrated with a Si optical waveguide (WG). The critical layer thickness for the pseudomorphic epitaxial growth is as low as <10 nm due to a large lattice mismatch of 4.2%, whereas a high-quality Ge layer is grown on Si using low–high-temperature two-step growth (typically, 350°C/600°C), followed by post-growth annealing at a high temperature of 800°C–900°C [26]. An important feature of such a Ge layer is its in-plane tensile lattice strain of about 0.2% [4–6]. A tensile strain, rather than a compressive strain due to the lattice mismatch, is induced after the cooling from the growth/annealing temperature to room temperature (RT) by a thermal expansion mismatch between the Ge layer and Si base substrate [27]. The tensile strain narrows the direct bandgap from 0.80 to ~0.77 eV, extending the fundamental optical absorption edge from 1.55 to ~1.61 µm in wavelength. This red shift helps increase the photodetection efficiency at 1.55 µm, or in the C band (1.530–1.565 µm) [4–6]. A Ge electroabsorption optical intensity modulator (EAM) [28], based on the Franz-Keldysh effect, is also a crucial device in terms of a significant reduction in the energy consumption over a Si-based electrooptic modulator. EAMs of elemental Ge on Si [29,30] showed an operating wavelength at around the absorption edge of 1.61 µm, or in the L band (1.565–1.625 µm), except for our recent work [31] on a submicron-wide Ge strip, where a C band modulation was obtained due to a strain relaxation effect presented in this study. For the C band modulation, a Ge/SiGe quantum well structure [32] or a wider-gap SiGe alloy with a Si composition as low as 1% [28,33–36] is generally required. However, similar to PD, elemental Ge is preferred to combine the Ge growth for PDs and EAMs into a single step. For a C band EAM, the direct bandgap of Ge, narrowed under the tensile strain, should be restored by the strain relaxation. A strip structure of Ge is probably effective, where edge-induced strain relaxation occurs, similar to the strip structure of compressive SiGe lattice-matched to Si [37]. Our group recently reported a gap restoration as a blue shift of about 10 nm in the photoluminescence (PL) peak when the Ge strip was narrowed to 2 µm [38]. A narrower submicron strip should achieve an enhanced blue shift required for a C band EAM. Such a submicron strip has recently played a significant role in PDs with operating frequencies higher than 50 GHz [22–25]; however, there has been no discussion on the strain relaxation effect. A recent study in ref. [36] used a strip structure of Ge-rich SiGe to control the operating wavelength of an EAM, but the focus is on the control of external stress applied by neighboring SiN_x layers.

Manuscript received May 31, 2022; revised July 26, 2022. This work was supported in part by "R&D on optical PLL device for receiving and monitoring optical signals," the Commissioned Research of National Institute of Information and Communication Technology, Japan (Grant No. 18101), by the JSPS KAKENHI (Grant No. JP21H01367), and by the Casio Science Promotion Foundation.

Shuhei Sonoi, Riku Katamawari, Manami Shimokawa, Kyosuke Inaba, Jose A. Piedra-Lorenzana, and Takeshi Hizawa are with the Department of Electrical and Electronic Information Engineering, Toyohashi University of Technology, Toyohashi 441-8580, Japan. (e-mail: sonoi.shuhei.sv@tut.jp; katamawari.riku.td@tut.jp; shimokawa.manami.eq@tut.jp; inaba.kyosuke.ro@tut.jp; piedra.lorenzana.jose.alberto.ei@tut.jp; hizawa@ts.tut.ac.jp).

Junichi Fujikata is with the Photonics Electronics Technology Research Association (PETRA), Tsukuba 305-8569, Japan. He is currently with the Graduate School of Sciences and Technology for Innovation, Tokushima University, Tokushima 770-8506, Japan (e-mail: fujikata.junichi@tokushima-u.ac.jp).

Yasuhiko Ishikawa is with the Department of Electrical and Electronic Information Engineering, Toyohashi University of Technology, Toyohashi 441-8580, Japan. (e-mail: ishikawa@ee.tut.ac.jp).

This study presents the bandgap engineering for an epitaxial layer of elemental Ge on Si toward the C+L band operation of EAMs and PDs, with the use of a narrow submicron strip structure, rather than wider-gap SiGe and narrower-gap GeSn alloys. Despite well-developed C band detection and L band modulation, the main goal is to achieve a C band modulation and improved L band detection. Significant blue shifts in PL and photodetection spectra of a narrow Ge strip are reported in Section IV after a theoretical analysis of the edge-induced strain relaxation in Section II and experimental procedures in Section III. A SiN_x standard external stressor was also studied, in which an increased blue shift or an opposite red shift is efficiently induced in a narrow strip, depending on the stress polarity in SiN_x. The results reveal the possibility of tuning the operating wavelength of EAMs and PDs of elemental Ge in the C+L band, as concluded in Section V.

II. Simulations of Lattice Strain and Absorption Spectrum in a Ge Strip Structure

A. Lattice Strain

Distributions of stress/lattice strain were simulated using a finite element method to study the edge-induced strain relaxation in a narrow strip of Ge. Similar to the experiments shown later, the thicknesses of the Ge strip and Si substrate were set to 0.5 and 525 μm, respectively, while the strip width was changed from 1 to 10 μm as a parameter. The strip edge was assumed to consist of inclined facet planes, based on experimental results. The structure was cooled from the Ge growth temperature of 700°C to RT (25°C), generating a tensile stress/strain in Ge by the thermal expansion mismatch. There was no strain due to the lattice mismatch before the cooling due to the Ge thickness of 0.5 μm, which was substantially larger than the critical layer thickness. In the simulation, the thermal expansion coefficient, α_{TE}, Young's modulus, Y, and Poisson's ratio, ν, were 5.9×10^{-6} K^{-1}, 103 GPa, and 0.26 for Ge, respectively, and 2.6×10^{-6} K^{-1}, 170 GPa, and 0.28, respectively, for Si. The Si surface, outside the Ge strip, was covered with a 0.1-μm-thick SiO_2 layer as a mask for the selective Ge growth. α_{TE}, Y, and ν were 5.5×10^{-7} K^{-1}, 73.1 GPa, and 0.17, respectively, for SiO_2.

Fig. 1 shows typical distributions of lattice strain at the cross-section of a sufficiently long Ge strip. Fig. 1(a) for a 10-μm-wide strip shows that a tensile lattice strain in the x (width) direction, ε_x, was as large as 0.20% at the strip center, which was similar to ε_y of 0.22% in the y (length) direction (Fig. 1(b)). The value of about 0.2% is consistent with the experimental value for a Ge film [4–6]. A compressive strain, ε_z, of about −0.15% was present in the z (thickness) direction, which was counter to the lattice tension in the x and y directions. Importantly, ε_x in Fig. 1(a) decreased toward the edge due to the edge-induced relaxation [37]. More significant relaxation occurs for a 1-μm-wide strip in Fig. 1(d), i.e., ε_x was almost relaxed within the strip. No such strain relaxation was observed in the length direction because of the absence of the edge in this direction. Thus, ε_y of 0.22% was maintained independent of the Ge width, as in Fig. 1(e). On the other hand, the absolute value of ε_z slightly decreased with narrowing the strip (Fig. 1(f)). This behavior is reasonable because the tensile strain/stress decreased in x direction.

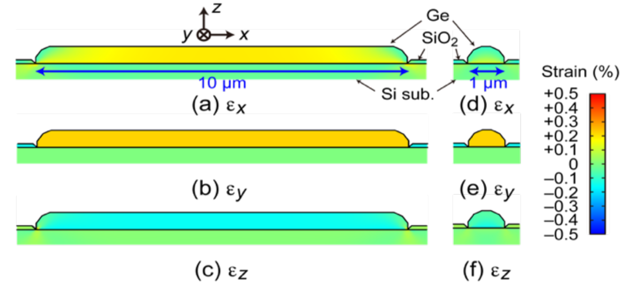

Fig. 1. Typical distributions of lattice strain in the x, y, and z directions for a 10-μm-wide Ge strip ((a) to (c)) and a 1-μm-wide Ge strip ((d) to (f)).

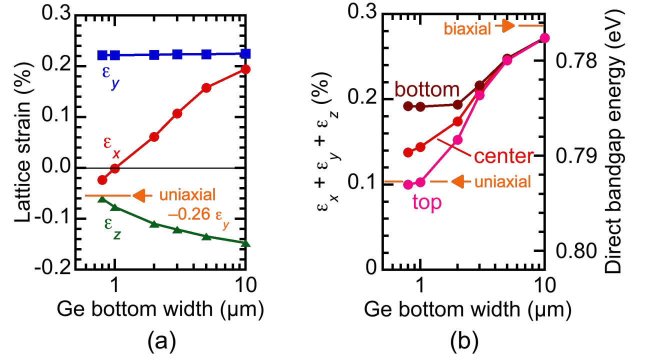

Fig. 2. (a) Lattice strains ε_x, ε_y, and ε_z at the center of a Ge strip and (b) the sum $\varepsilon_x + \varepsilon_y + \varepsilon_z$ at different locations in the vertical direction as a function of the bottom width of a Ge strip.

The strains of ε_x, ε_y, and ε_z at the strip center are plotted in Fig. 2(a) as a function of the bottom width of the Ge strip. ε_x and ε_z approached to $-\nu\varepsilon_y$ ($\nu = 0.26$) when the strip is narrowed as small as 1 μm or below. This indicates approximately uniaxial stress, in contrast to biaxial stress in a wide strip. The sum, $\varepsilon_x + \varepsilon_y + \varepsilon_z$, corresponding to the volume change, $\Delta V/V$, is plotted in Fig. 2(b) at different locations in the z direction, i.e., at the top bare surface, bottom interface with Si, and the center, although the optical power in an EAM/PD of a Ge strip should be higher around the center [31]. The right axis shows an estimate of the direct bandgap energy, which was determined using the following relationship [39]:

$$E_g \sim E_{g0} + a(\varepsilon_x + \varepsilon_y + \varepsilon_z), \quad (1)$$

where E_{g0} and a are the direct bandgap energy of unstrained Ge (0.802eV at RT [40]) and the dilation deformation potential of Ge (−8.97 eV [41]), respectively. The ideal values of $\varepsilon_x + \varepsilon_y + \varepsilon_z$ for the biaxial and uniaxial stresses are indicated in Fig. 2(b), which are expressed as $[2 - 2\nu/(1-\nu)]\varepsilon_y$ and $(1-2\nu)\varepsilon_y$, respectively. Fig. 2(b) shows that the strain was more relaxed at the top surface, approximately corresponding to uniaxial stress for a strip of <1 μm in width. A significant strain relaxation was also observed at the center and even at the bottom interface. The direct gap energy at the strip center was restored from 0.778 to 0.789 eV for the 1-μm-wide strip, corresponding to the optical absorption edge from 1.594 to 1.572 μm in wavelength, or a blue shift of more than 20 nm.

B. Bandgap Energy and Optical Absorption Spectrum

The direct gap energy was more precisely analyzed, considering the splitting between the light-hole (LH) and heavy-hole (HH) valence bands under nonhydrostatic stress [39]. The relationship between the crystallographic and stress directions is critical; a quasi-uniaxial [110] stress is applied to a submicron Ge strip ordinarily aligned in the [110] direction. Shear components in the lattice strain are present, enhancing the valence band splitting [42,43]. Fig. 3 shows the direct bandgap energies between the conduction (C) and LH/HH valence bands, calculated as a function of the stress in a (001) Ge layer. The deformation potentials in refs. [41] and [44] were used, and the uniaxial [110] stress was compared with the biaxial stress. The biaxial tensile strain of 0.20% corresponds to the in-plane stress of 0.28 GPa using elastic constants of c_{11} = 128.5 GPa and c_{12} = 48.3 GPa for Ge. The same stress of 0.28 GPa should be uniaxially applied for a narrow strip. Fig. 3 shows that both the C-LH and C-HH gaps under the [110] uniaxial stress (0.784 and 0.798 eV, respectively, at 0.28 GPa) were wider than those for the biaxial one (0.773 and 0.786 eV, respectively). Particularly, the C-HH gap energy under the [110] uniaxial stress was 0.798 eV, which was comparable to the unstrained one of 0.802 eV, shifting the absorption edge to 1.554 µm in the C band.

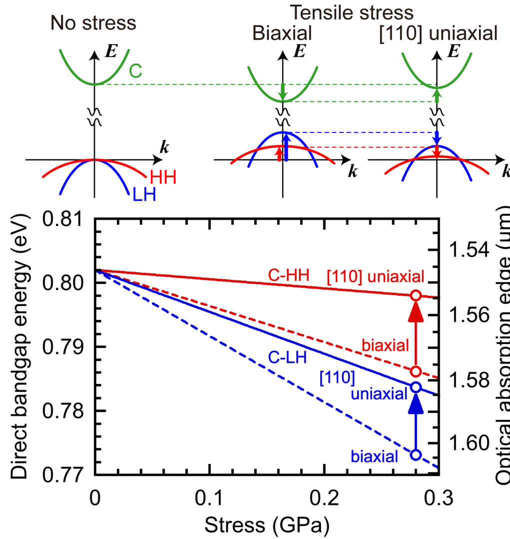

Fig. 3. Direct bandgap energies as a function of stress applied to (001) Ge under biaxial (dashed lines) and [110] uniaxial (solid lines) stresses. The changes in the conduction and LH/HH valence bands are schematically shown at the top.

Fig. 4 shows optical absorption spectra of Ge under several applied electric fields (0–100 kV/cm), which were theoretically calculated in the C and L bands for the biaxial and [110] uniaxial stresses (0.28 GPa). A formula of the absorption coefficient α as a function of the photon energy E in ref. [45] was used, considering the Frantz-Keldysh effect, i.e.,

$$\alpha(E) = (A_0/2\pi)(2m_r/\hbar^2)^{3/2}\sqrt{\hbar\theta_F}[-\eta Ai^2(\eta) + Ai'^2(\eta)], \quad (2a)$$

$$A_0 = (\pi\hbar e^2 E_p)/(6n_r c\varepsilon_0 m_0 E), \quad (2b)$$

$$\hbar\theta_F = [(\hbar^2 e^2 F^2)/(2m_r)]^{1/3}, \quad (2c)$$

and

$$\eta = (E_g - E)/\hbar\theta_F. \quad (2d)$$

Here, $Ai(\eta)$ and $Ai'(\eta)$ are the Airy function and its derivative, respectively. m_r is the interband reduced mass, $\hbar$ the reduced Planck constant, e the elementary charge, E_p the optical matrix energy parameter, n_r the refractive index, c the speed of light, ε_0 the permittivity in vacuum, m_0 the electron rest mass, F the electric field strength, and E_g the direct bandgap energy. The absorption coefficients are given by the summation of two components of the C-HH and C-LH transitions. The interband reduced masses are $0.0330m_0$ for the C-HH transition and $0.0195m_0$ for the C-LH transition [46]. E_p and n_r were 26.3 eV and 4.0, respectively [46].

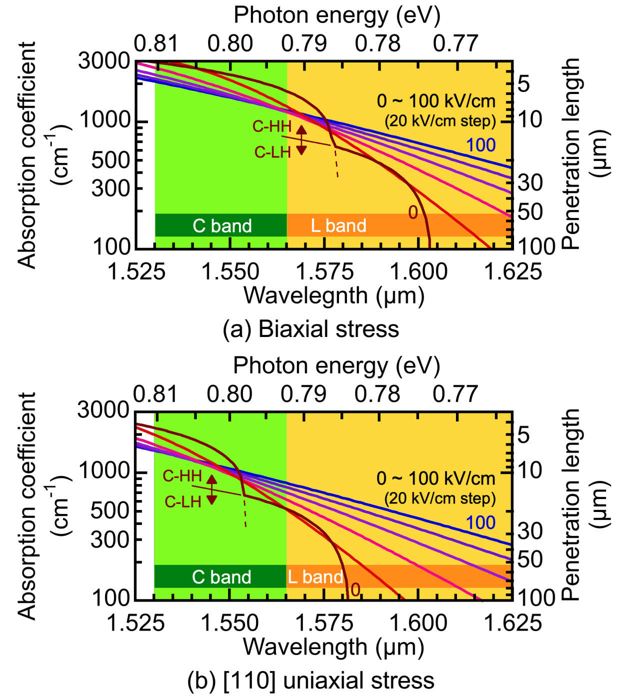

Fig. 4. Spectra of the optical absorption coefficient under different applied electric fields for (a) biaxial stress and (b) [110] uniaxial stress (0.28 GPa).

At 0 kV/cm, an inflection point was observed at the photon energy equal to the C-HH gap energy due to a superposition of two components of the C-LH and C-HH transitions; the C-HH transitions dominated the absorption coefficient in the shorter wavelength region, reflecting the higher optical density of states [5,46]. In the biaxial case of Fig. 4(a), the absorption coefficient increased under the electric field at wavelengths approximately longer than 1.578 µm, corresponding to the C-HH gap energy of 0.786 eV. This implies that the biaxially strained Ge applies to an EAM operating in a wide range of the L band, despite background absorption up to ~1.60 µm due to the C-LH transitions. The biaxially strained Ge also applies to a PD up to ~1.60 µm, whereas enhanced absorption under the electric field would support a PD operation in the entire L band [19]. Alternatively, the absorption spectra in the uniaxial case of Fig. 4(b) were shifted toward the shorter wavelength. An enhanced absorption due to the Franz-Keldysh effect appears at >1.554 µm, indicating applicability to an EAM operating in a part of the C band. As shown later, a bandgap widening induced by an external stressor of SiN_x can increase the blue shift, potentially achieving an EAM operating in the entire C band. A

red shift is also possible by changing the stress polarity of SiN_x, resulting in improved L band detection.

III. Preparation of Ge Strip Structures and Characterization Methods

A. Selective Epitaxy of the Ge Strip Structure on Si

The strip narrowing effects were experimentally investigated. 4-inch (001) Si wafers were used as the starting substrate, on which a 100-nm-thick SiO_2 layer was formed via thermal oxidation. The SiO_2 layer was partly removed to open strip-shaped windows of the exposed Si surface in the [110] direction. As a parameter, the window width was changed from 0.9 (±0.1) to 100 μm, while the length was sufficiently long (>1 mm). A Ge epitaxial layer was selectively grown on the Si windows via ultrahigh-vacuum chemical vapor deposition (CVD) using a source gas of 9% GeH_4 in Ar [46–48]. A two-step growth method [26] was used, in which a 50-nm-thick Ge buffer layer was grown at a low temperature of 370°C, followed by Ge growth at an elevated temperature of 700°C. The Ge thickness was designed to be 500 nm. The effect of a standard SiN_x external stressor was also studied in terms of further controlling the direct bandgap. SiN_x was deposited on the Ge strip surface as an overlayer using plasma-enhanced CVD. 10%-SiH_4/N_2, NH_3, and N_2 gases were supplied with a flow-rate ratio of 39:2:61 at an RF power of 100 W [49]. The sample temperature was 300°C, and two different chamber pressures of 200 and 50 Pa were used, resulting in SiN_x film stresses of +0.60 GPa (tensile) and −0.15 GPa (compressive), respectively. The thicknesses were approximately 500 and 400 nm for the tensile and compressive SiN_x layers, respectively.

B. Characterization Methods

Scanning electron microscopy (SEM) was used for the structural characterization. The Raman spectra were measured at RT using a 457-nm laser source and an arrayed Si detector to evaluate the strain relaxation [50]. The laser power and nominal $1/e^2$ spot diameter at the sample surface were 1.0 mW and 1 μm, respectively. The $1/e$ penetration depth in Ge is approximately 20 nm, which measures the near-surface region. PL spectra were measured at RT in the wavelength range of 1.4–1.7 μm to evaluate the bandgap energy [50]. A 785-nm laser was used as the excitation source. The laser power and nominal $1/e^2$ spot diameter were 4.0 mW and 2 μm, respectively. The $1/e$ penetration depth in Ge was approximately 100 nm. Further, to directly confirm the narrowing effect, photodetection spectra were measured for lateral pin PDs of a selectively grown Ge strip integrated with a Si WG on a Si-on-insulator (SOI) platform. The device was used as an EAM in ref. [31]. As shown later in detail, the device was composed of a rib-like (strip-loaded) structure of a Ge strip on a Si pedestal of SOI. Three different widths of the strip were prepared (0.5, 0.8, and 1.2 μm at the bottom, denoted in ref. [31] as nominal widths of 0.3, 0.6, and 1.0 μm, respectively) with a length of 40 μm. Concerning the single-mode light propagation for an EAM, the Ge height was reduced to approximately 200 nm, although a thicker strip should be preferable in terms of the edge-induced strain relaxation. A lensed fiber was used to couple the TE-polarized light from a tunable laser source (1.455–1.640 μm) to the Si WG via a spot-size converter at the edge of the chip. The coupling loss was approximately −7 dB. The sample temperature was thermo-electrically controlled at 30°C.

IV. Experimental Results and Discussions

A. Structural Characterizations by SEM

Fig. 5 summarizes typical cross-sectional SEM images of Ge strips selectively grown on Si. Fig. 5(a) shows that, for a relatively wide strip with a bottom width of 5.5 μm, a mesa structure was formed, consisting mainly of a (001) surface at the top and an inclined {113} facet sidewall, which is similar to previous works [1,48]. The {113} facet sidewalls usually appear because of the low growth rate on the {113} plane [51]. The sidewall was more inclined than the 10-μm-wide strip in the simulation (Fig. 1) because the {113} facet dominated the sidewall. A small facet was observed at the bottom edge, approximately corresponding to the {112} plane rather than the {111} plane [48]. The strip thickness at the center was 470 nm, which is consistent with the 500-nm designed thickness. A mound was observed near the sidewall, probably resulting from the migration of Ge atoms from the facet sidewalls. The largest thickness at the mound was 530 nm.

The area of the (001) top surface was reduced by narrowing the strip. The thickness/height of Ge for the 2.5-μm-wide strip in Fig. 5(b) was almost equal to 530 nm at the mound in Fig. 5(a). When the strip was further narrowed to 1.5 μm, {111} planes appeared as a sidewall facet adjacent to the {113} plane (Fig. 5(c)). Vertical {110}-like facets were also observed near the bottom edge for the narrowest 0.9-μm-wide strip in Fig. 5(d), which was similar to the structure in the simulation (Fig. 1). The plane was slightly inclined at ~6° from the vertical direction, nominally corresponding to the {771} plane [48]. The Ge height decreased to 400 and 370 nm for strip widths of 1.5 and 0.9 μm, respectively. Athough the surface was microscopically composed of the facet planes, the Ge strip in Fig. 5(d) was close to a semicylindrical shape, probably minimizing in the surface energy (surface area). Figs. 6(a) and (b) show typical images after the deposition of a SiN_x layer with tensile (+0.60 GPa) and compressive (−0.15 GPa) stresses, respectively. In both cases, a SiN_x layer uniformly covered the Ge strip.

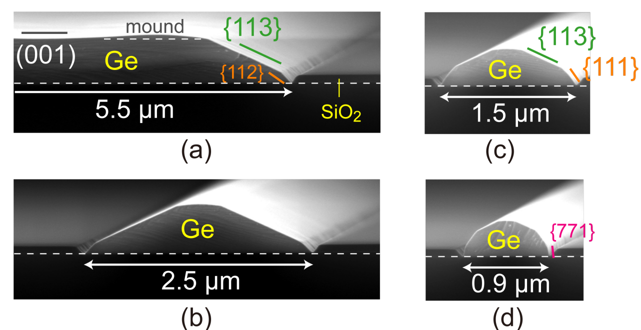

Fig. 5. Typical SEM images of Ge strip structures selectively grown on Si with bottom widths of (a) 5.5 μm, (b) 2.5 μm, (c) 1.5 μm, and (d) 0.9 μm.

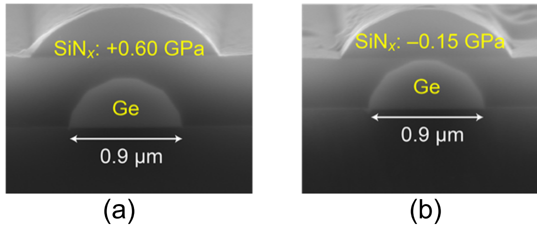

Fig. 6. Typical SEM images of a 0.9-µm-wide Ge strip structure on Si covered with a SiN_x layer possessing (a) tensile and (b) compressive stresses.

B. Raman Spectra

Fig. 7 summarizes the Raman spectra for different widths of the strip without SiN_x overlayer. The dots correspond to the experimental data points, whereas the lines correspond to the fitting curves with the Lorentzian function. The vertical lines indicate the peak positions based on the fitting. As a reference, a spectrum from an unstrained (001) bulk Ge wafer is shown at the bottom. A peak was observed at around 300 cm^{-1} in each spectrum, corresponding to the Ge–Ge bonding in Ge. For the 100-µm-wide Ge at the top of Fig. 7, a negative shift of $\Delta\omega \sim -0.7$ cm^{-1} was observed compared with the peak from the bulk Ge. The shift is attributed to a biaxial tensile strain, $\varepsilon_{\parallel}$, which is estimated to be 0.16% using the following relationship [52]

$$\varepsilon_{\parallel}\,(\%) = -0.23 \times \Delta\omega\,(\mathrm{cm}^{-1}). \quad (3)$$

The strain of 0.16% is consistent with the reported one of around 0.2% in a Ge film [4–6]. The 10-µm-wide strip showed almost the same $\Delta\omega$ as that in the 100-µm case, whereas the negative shift was gradually reduced as the strip was narrowed below 10 µm, which corresponds to strain relaxation. The narrowing shift is not due to heating caused by high laser excitation, which results in a negative Raman peak shift [53].

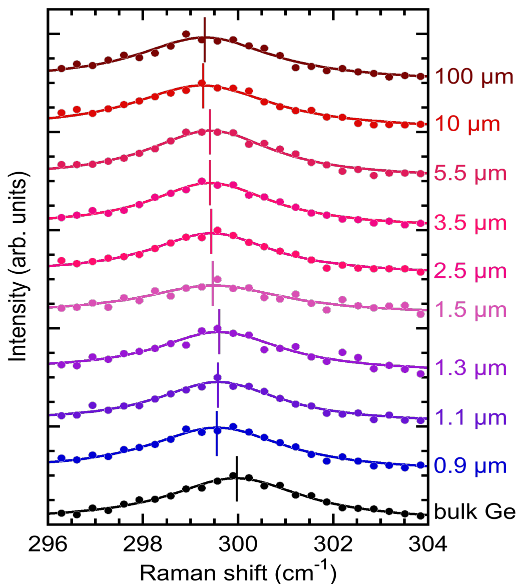

Fig. 7. Typical Raman spectra at RT obtained for Ge strips (without a SiN_x overlayer) with different widths.

Fig. 8 shows the plot of the Raman peak position as a function of the width of the Ge strip. The negative shift was reduced to $\Delta\omega \sim -(0.3–0.4)$ cm^{-1} when the strip was narrowed to as small as 1 µm, which is almost a half of -0.7 cm^{-1} for the 100-µm case. This is logical because the tensile strain should be relaxed in the width direction, whereas no strain relaxation occurs in the length direction, as shown in Fig. 2(a).

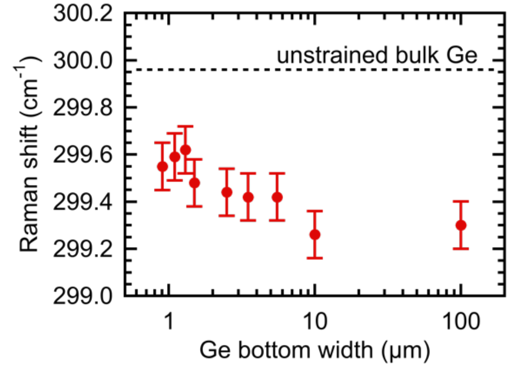

Fig. 8. Raman peak positions as a function of the bottom width of Ge.

C. PL Spectra

Fig. 9(a) summarizes the PL spectra for different widths of the strip without SiN_x. As shown at the bottom of the figure, an unstrained (001) bulk Ge reference revealed a PL peak at around 1.55 µm, corresponding to a photon energy of 0.80 eV. This value is consistent with the direct bandgap energy for unstrained Ge [40], implying that the observed PL emission is attributed to the direct band-to-band transitions. The peak was asymmetric, showing a tail toward the shorter wavelength. This is probably attributed to excited electrons and holes energetically distributed in the conduction and valence bands. The central wavelengths at the half maximum are indicated by dots due to the peak asymmetry. For the 100-µm-wide Ge at the top, the PL peak was located at a wavelength approximately 30-nm longer than that of the bulk Ge. The presence of a tensile strain is qualitatively confirmed by this red shift. For $\varepsilon_{\parallel} \sim 0.16\%$ (the biaxial stress of 0.23 GPa), the theoretical C-HH and C-LH gap energies are 0.789 and 0.779 eV, respectively (Fig. 3). These energies correspond to the wavelengths of 1.572 and 1.592 µm, respectively, implying that the observed PL emission is dominated by the C-HH transitions, with the optical density of states higher than that for C-LH. The PL red shift was gradually reduced when the strip was narrowed below 10 µm due to the strain relaxation, as observed in Figs. 7 and 8. The heating effect caused by the laser excitation is not responsible for the reduced red shift since heating reduces the gap energy [40]. The central wavelength of the PL emission for a strip as narrow as 1 µm approached that of the unstrained Ge, making it useful for an EAM to shorten the operating wavelength toward the C band. However, the comparison of the central wavelength probably overestimated the effect of the strip narrowing because the highest PL intensity for the 0.9-µm strip was ~10-nm longer than that for the bulk Ge.

In Fig. 9(b), the central wavelengths were plotted as a function of the bottom width of Ge. The wavelengths corresponding to the bandgap energies estimated in Fig. 2(b) are also shown. Although the PL central wavelengths were approximately 30 nm shorter than theoretical ones from Fig. 2(b), the amount of the wavelength shift with the strip narrowing revealed a good agreement between the PL and theoretical results. To directly and accurately confirm the

spectral shift with narrowing the Ge strip, the absorption spectra of pin PDs with different strip widths are evaluated in the next section.

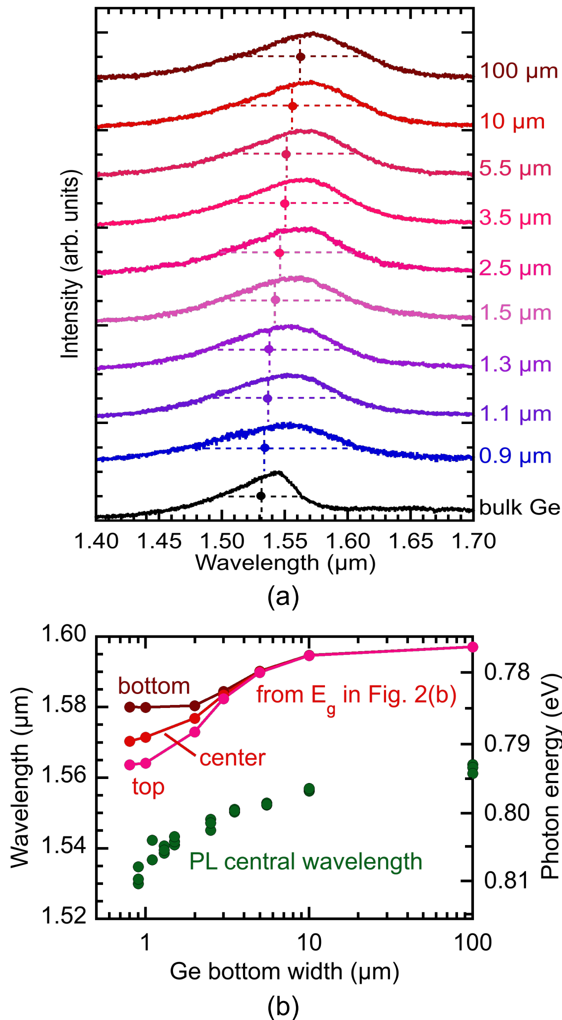

Fig. 9. (a) PL spectra at RT obtained for Ge strips (without a SiN_x overlayer) with different widths, and (b) central wavelengths at the half maximum of the PL peak as a function of the bottom width of Ge. In (b), the wavelengths corresponding to the estimated bandgap energies in Fig. 2(b) are also shown.

Fig. 10(a) summarizes the effect of the SiN_x overlayer on the PL spectrum. The results were compared among the second-narrowest 1.1-μm-wide strips because the narrowest 0.9-μm strip exhibited a significantly low PL intensity in the case of the tensile SiN_x overlayer, reflecting that the resultant direct gap widening is unfavorable for PL emission from Ge. After depositing SiN_x with tensile stress, which should provide compressive stress to the underlying Ge strip, the peak was shifted toward the shorter wavelength compared with the PL peak for a Ge strip without SiN_x. In contrast, a red shift was observed when SiN_x was subjected to compressive stress. No such shift was observed in the case of a sufficiently wide strip (100 μm, not shown). This is reasonable because a narrow structure is required for both the edge-induced strain relaxation and an efficient application of external stress. Fig. 10(b) summarizes the central wavelength of the PL emission as a function of the Ge width. Compared with the strip without SiN_x, the deposition of a tensile SiN_x layer revealed a blue shift as large as 20 nm for a strip as narrow as 1 μm. This implies that an EAM of a narrow strip can operate in the entire C band by optimizing the SiN_x stressor technique. The compressive SiN_x deposition revealed a red shift up to 1.58 μm, which is even about 20-nm longer than the 1.56 μm for the 100-μm-wide Ge. The L band photodetection could be efficiently improved.

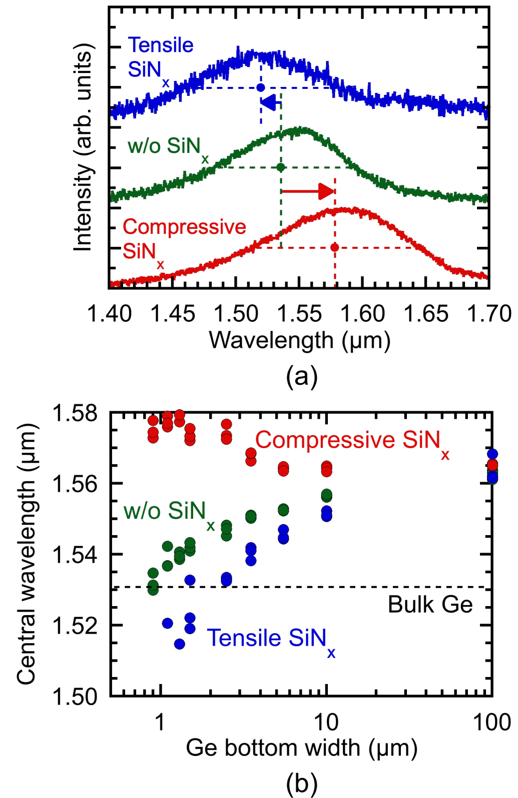

Fig. 10. (a) Typical PL spectra from the 1.1-μm-wide strip with and without a SiN_x overlayer, and (b) central wavelengths at the half maximum of the PL peak as a function of the bottom width of Ge.

D. *Optical Absorption Spectra*

Responsivity spectra for lateral pin PDs of a selectively grown Ge strip integrated with a Si WG were measured to observe the effect of strip narrowing more directly. As shown in Fig. 11(a), a strip-loaded structure of a Ge strip on a Si pedestal of SOI was used. In the fabrication, a lateral pin junction was formed in the SOI layer by phosphorus and boron implantations, followed by a patterning of the SOI layer to form a Si channel WG connected to the Si pedestal. Then, a selective growth of a Ge strip (approximately 200 nm in thickness) was performed on the Si pedestal with a SiO_2 mask. After phosphorus and boron implantations at the sidewalls of the Ge strip, an overcladding layer of SiO_2 was deposited. Finally, Al/Ti contanct electrodes were formed. More details are described in ref. [31]. Fig. 11(b) shows typical responsivity spectra of 40-μm-long Ge PDs with different strip widths of 0.5, 0.8, and 1.2 μm. Here the spectra were taken at 0 V to minimize the Franz-Keldysh effect. The noisy spectra for the 0.8- and 1.2-μm devices were derived from Fabry-Perot resonances because the wavelength positions of the fluctuations were well reproduced in the repeated measurements. The responsivity at the shortest wavelength of

about 1.46 μm was as large as 0.2 A/W, which was almost independent of the Ge width. This value corresponds to approximately 1.0 A/W when subtracting the coupling loss of −7 dB, indicating a quantum efficiency as high as 80%. The responsivity of the 1.2-μm strip decreased above 1.56 μm, whereas that of the 0.8- and 0.5-μm strips started to decrease at shorter wavelengths of about 1.53 and 1.50 μm, respectively. This is direct evidence of a blue shift in the optical absorption spectrum with the narrowing of the strip.

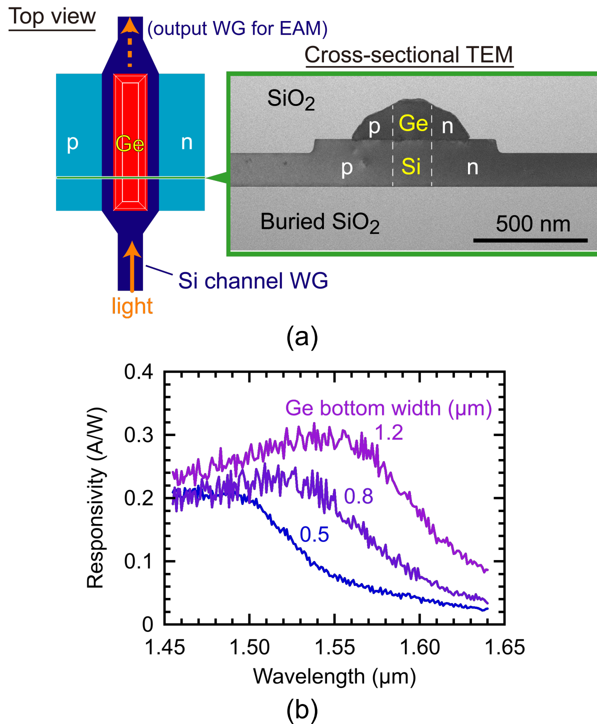

Fig. 11. (a) A schematic top view of a lateral pin PD of a Ge strip and a typical cross-sectional transmission electron microscope (TEM) image for the Ge bottom width of 0.5 μm, and (b) typical responsivity spectra at 30°C.

The responsivity of the 0.5-μm-wide strip was significantly low at around 1.55 μm. This suggests an EAM of elemental Ge operating in the C band, in contrast to the wider-gap SiGe alloy used in previous studies [28,33–36]. The same device has been found to operate as an EAM in the C band, as reported in ref. [31]. On the other hand, the 1.2-μm-wide strip revealed a high responsivity in the C band, i.e., a wider strip is appropriate for a PD in the C band. This implies that the Ge growth for PDs and EAMs in the C band can be merged into a single step, favorably simplifying the process steps for their integration. There is still an issue for the 0.5-μm strip, such that the low responsivity at around 1.55 μm appears to contradict the large optical absorption coefficient (>1000 cm^{-1}) in the calculated result in Fig. 4(b). A compressive strain may be applied by a SiO_2 over-cladding layer to cause a blue shift. A wider-gap SiGe alloy formed accidentally during the annealing process may also be responsible for a blue shift; however, more research is needed to clarify this point. No special band engineering, except for the strip width control, is required for an EAM in terms of the L band operation, whereas the deposition of compressive SiN_x is useful for PDs to enhance optical absorption in the L band and potentially in the U band of 1.625–1.675 μm. In fact, the present PL result in Fig. 10(a) showed a significant emission intensity in the U band, suggesting a potential photodetection. The Franz-Keldysh effect should also be effective for PDs in the entire L band [19]. An enhanced responsivity in the L and U bands has been experimentally obtained by applying a reverse bias to the PDs used in Fig. 11; however, the detailed spectral responsivity under the reverse bias will be described elsewhere. The current results on the narrow strip show the possibility of tuning the operating wavelength of EAMs and PDs of elemental Ge in the C+L band.

V. Conclusions

Bandgap engineering was presented for a Ge epitaxial layer on Si to tune the operating wavelength of EAMs and PDs in the C+L band, without the use of SiGe and GeSn alloys. The key concept is to use a strip structure of Ge; a tensile lattice strain in Ge is relaxed by narrowing the strip to the submicron scale, restoring the narrowed bandgap of ~0.77 eV toward 0.80 eV of unstrained Ge. A significant blue shift was observed in the PL peak and photodetection spectra. A SiN_x stressor also caused an increased blue shift or an opposite red shift. The results show the possibility of tuning the operating wavelength of Ge EAMs and PDs in the C+L band, combining the Ge growth for the devices into a single step.

Acknowledgment

The authors would like to thank Michiharu Nishimura and Kazuki Kawashita for their experimental supports and the Photonics Electronics Technology Research Association for supplying the PD samples.

References

[1] J. Michel, J. Liu, and L. C. Kimerling, “High-performance Ge-on-Si photodetectors,” *Nat. Photon.*, vol. 4, no. 8, pp. 527–534, Aug. 2010.

[2] G. Masini, L. Colace, G. Assanto, H. -C. Luan, and L. C. Kimerling, “High-performance p-i-n Ge on Si photodetectors for the near infrared: from model to demonstration,” *IEEE Trans. Electron Devices*, vol. 48, no. 6, pp. 1092–1096, Jun. 2001.

[3] Y. Ishikawa, K. Wada, D. D. Cannon, J. Liu, H. -C. Luan, and L. C. Kimerling, “Strain-induced band gap shrinkage in Ge grown on Si substrate,” *Appl. Phys. Lett.*, vol. 82, no. 13, pp. 2044–2046, Mar. 2003.

[4] J. Liu, J. Michel, W. Giziewicz, D. Pan, K. Wada, D. D. Cannon, S. Jongthanmmanurak, D. T. Danielson, L. C. Kimerling, J. Chen, F. Ömer Ilday, F. X. Kärtner, and J. Yasaitis, “High-performance, tensile-strained Ge p-i-n photodetectors on a Si platform,” *Appl. Phys. Lett.*, vo. 87, no. 10, Sep. 2005, Art. no. 103501.

[5] Y. Ishikawa, K. Wada, D. D. Cannon, J. Liu, H. -C. Luan, J. Michel, and L. C. Kimerling, “Strain-induced enhancement of near-infrared absorption in Ge epitaxial layers grown on Si substrate,” *J. Appl. Phys.*, vol. 98, no. 1, Jul. 2005, Art. no. 013501.

[6] M. Jutzi, M. Berroth, G. Wöhl, M. Oehme, and E. Kasper, “Ge-on-Si vertical incidence photodiodes with 39-GHz bandwidth,” *IEEE Photon. Technol. Lett.*, vol. 17, no. 7, pp. 1510–1512, Jul. 2005.

[7] D. Ahn, C. -Y. Hong, J. Liu, W. Giziewicz, M. Beals, L. C. Kimerling, and J. Michel, “High performance, waveguide integrated Ge photodetectors,” *Opt. Express*, vol. 15, no. 7, pp. 3916–3921, Apr. 2007.

[8] T. Yin, R. Cohen, M. M. Morse, G. Sarid, Y. Chetrit, D. Rubin, and M. J. Paniccia, “31 GHz Ge n-i-p waveguide photodetectors on silicon-on-insulator substrate,” *Opt. Express*, vol. 15, no. 21, pp. 13965-13971, Oct. 2007.

[9] G. Masini, S. Sahni, G. Capellini, J. Witzens, and C. Gunn, "High-speed near infrared optical receivers based on Ge waveguide photodetectors integrated in a CMOS process," *Adv. Opt. Technol.*, vol. 2008, Jun. 2008, Art. no. 196572.

[10] L. Vivien, J. Osmond, J. -M. Fédéli, D. Marris-Morini, P. Crozat, J. -F. Damlencourt, E. Cassan, Y. Lecunff, and S. Laval, "42 GHz pin Germanium photodetector integrated in a silicon-on-insulator waveguide," *Opt. Express*, vol. 17, no. 8, pp. 6252–6257, Apr. 2009.

[11] K. -W. Ang, T. Y. Liow, M. B. Yu, Q. Fang, J. Song, G. Q. Lo, and D. L. Kwong, "Low thermal budget monolithic integration of evanescent-coupled Ge-on-SOI photodetector on Si CMOS platform," *IEEE J. Select. Topics Quantum Electron*., vol. 16, no. 1, pp. 106–113, Jan./Feb. 2010.

[12] N. -N. Feng, P. Dong, D. Zheng, S. Liao, H. Liang, R. Shafiiha, D. Feng, G. Li, J. E. Cunningham, A. V. Krishnamoorthy, and M. Asghari, "Vertical p-i-n germanium photodetector with high external responsivity integrated with large core Si waveguides," *Opt. Express*, vol. 18, no. 1, pp. 96–101, Jan. 2010.

[13] S. Park, T. Tsuchizawa, T. Watanabe, H. Shinojima, H. Nishi, K. Yamada, Y. Ishikawa, K. Wada, and S. Itabashi, "Monolithic integration and synchronous operation of germanium photodetectors and silicon variable optical attenuators," *Opt. Express*, vol. 18, no. 8, pp. 8412–8421, Apr. 2010.

[14] G. Li, Y. Luo, X. Zheng, G. Masini, A. Mekis, S. Sahni, H. Thacker, J. Yao, I. Shubin, K. Raj, J. E. Cunningham, and A. V. Krishnamoorthy, "Improving CMOS-compatible germanium photodetectors," *Opt. Express*, vol. 20, no. 24, pp. 26345–26350, Nov. 2012.

[15] H. Nishi, T. Tsuchizawa, R. Kou, H. Shinojima, T. Yamada, H. Kimura, Y. Ishikawa, K. Wada, and K. Yamada, "Monolithic integration of a silica AWG and Ge photodiodes on Si photonic platform for one-chip WDM receiver," *Opt. Express*, vol. 20, no. 8, pp. 9312–9321, Apr. 2012.

[16] T. Hiraki, H. Nishi, T. Tsuchizawa, R. Kou, H. Fukuda, K. Takeda, Y. Ishikawa, K. Wada, and K. Yamada, "Si-Ge-Silica Monolithic Integration Platform and Its Application to a 22-Gb/s × 16-ch WDM Receiver," I*EEE Photonics J.*, vol. 5, no. 4, Aug. 2013, Art. no. 4500407.

[17] J. Fujikata, M. Miura, M. Noguchi, D. Okamoto, T. Horikawa, and Y. Arakawa, "Si waveguide-integrated metal–semiconductor–metal and p–i–n-type Ge photodiodes using Si-capping Layer," *Jpn. J. Appl. Phys.*, vol. 52, no. 4, Apr. 2013, Art. no. 04CG10.

[18] K. Yamada, T. Tsuchizawa, H. Nishi, R. Kou, T. Hiraki, K. Takeda, H. Fukuda, Y. Ishikawa, K. Wada, and T. Yamamoto, "High-performance silicon photonics technology for telecommunications applications," *Sci. Technol. Adv. Mater.*, vol. 15, no. 2, Apr. 2014, Art. no. 024603.

[19] K. Takeda, T. Hiraki, T. Tsuchizawa, H. Nishi, R. Kou, H. Fukuda, T. Yamamoto, Y. Ishikawa, K. Wada, and K. Yamada, "Contributions of Franz–Keldysh and Avalanche Effects to Responsivity of a Germanium Waveguide Photodiode in the L-band," *IEEE J. Select. Topics Quantum Electron.*, vol. 20, no. 4, Jul./Aug. 2014, Art. no. 3800507.

[20] C. G. Littlejohns, Y. Hu, F. Y. Gardes, D. J. Thomson, S. A. Reynolds, G. Z. Mashanovich, and G. T. Reed, "50 Gb/s silicon photonics receiver with low insertion loss," *IEEE Photon. Technol. Lett.*, vol. 26, no. 7, pp. 714–717, Apr. 2014.

[21] K. Ito, T. Hiraki, T. Tsuchizawa, and Y. Ishikawa, "Waveguide-integrated vertical pin photodiodes of Ge fabricated on p^+ and n^+ Si-on-insulator layers," *Jpn. J. Appl. Phys.*, vol. 56, no. 4, Apr. 2017, Art. no. 04CH05.

[22] H. Chen, M. Galili, P. Verheyen, P. De Heyn, G. Lepage, J. De Coster, S. Balakrishnan, P. Absil, L. Oxenlowe, J. Van Campenhout, and G. Roelkens, "100 Gbps RZ Data Reception in 67-GHz Si-Contacted Germanium Waveguide p-i-n Photodetectors," *J. Lightwave Technol.*, vol. 35, no. 4, pp. 722–726, Feb. 2017.

[23] L. Virot, D. Benedikovic, B. Szelag, C. Alonso-Ramos, B. Karakus, J. -M. Hartmann, X. L. Roux, P. Crozat, E. Cassan, D. Marris-Morini, C. Baudot, F. Boeuf, J. -M. Fédéli, C. Kopp, and L. Vivien, "Integrated waveguide PIN photodiodes exploiting lateral Si/Ge/Si heterojunction," *Opt. Express*, vol. 25, no. 16, pp. 19487–19496, Aug. 2017.

[24] F. Boeuf, A. Fincato, L. Maggi, J. F. Carpentier, P. Le Maitre, M. Shaw, S. Cremer, N. Vulliet, C. Baudot, S.Monfray, S. Jan, C. Deglise, J. R. Manouvrier, C. Durand, A. Simbula, D. Goguet, P. Bar, D. Ristoiu, F. Leverd, L. Babaud, A. Daverio, M.Binda, A. Bazzotti, A. Canciamilla, L. Ramini, M.Traldi, P. Gambini, "A Silicon Photonics Technology for 400 Gbit/s Applications," in *2019 Int. Electron Dev. Meeting (IEDM) Technical Digest*, 33.1.1.

[25] S. Lischke, A. Peczek, J. S. Morgan, K. Sun, D. Steckler, Y. Yamamoto, F. Korndörfer, C. Mai, S. Marschmeyer, A. Krüger, A. Beling, and L. Zimmermann, "Ultra-fast germanium photodiode with 3-dB bandwidth of 265 GHz," *Nat. Photon.*, vol. 15, no. 12, pp. 925–931, Dec. 2021.

[26] H. -C. Luan, D. R. Lim, K. K. Lee, K. M. Chen, J. G. Sandland, K. Wada, and L. C. Kimerling, "High-quality Ge epilayers on Si with low threading-dislocation densities," *Appl. Phys. Lett.,* vol. 75, no. 19, pp. 2909–2911, Nov. 1999.

[27] R. R. Reeber and K. Wang, "Thermal expansion and lattice parameters of group IV semiconductors," *Mater. Chem. Phys.*, vol. 46, no. 2-3, pp. 259–264, Nov. 1996.

[28] J. Liu, M. Beals, A. Pomerene, S. Bernardis, R. Sun, J. Cheng, L. C. Kimerling, and J. Michel, "Waveguide-integrated, ultralow-energy GeSi electro-absorption modulators," *Nat. Photon.*, vol. 2, no. 7, pp. 433–437, Jul. 2008.

[29] A. E. -J. Lim, T. -Y. Liow, F. Qing, N. Duan, L. Ding, M. Yu, G. -Q. Lo, and D. -L. Kwong, "Novel evanescent-coupled germanium electro-absorption modulator featuring monolithic integration with germanium p-i-n photodetector," *Opt. Express*, vol. 19, no. 6, pp. 5040–5046, Mar. 2011.

[30] N. -N. Feng, D. Feng, S. Liao, X. Wang, P. Dong, H. Liang, C. -C. Kung, W. Qian, J. Fong, R. Shafiiha, Y. Luo, J. Cunningham, A. V. Krishnamoorthy, and M. Asghari, "30GHz Ge electro-absorption modulator integrated with 3μm silicon-on-insulator waveguide," *Opt. Express*, vol. 19, no. 8, pp. 7062–7067, Apr. 2011.

[31] J. Fujikata, M. Noguchi, K. Kawashita, R. Katamawari, S. Takahashi, M. Nishimura, H. Ono, D. Shimura, H. Takahashi, H. Yaegashi, T. Nakamura, and Y. Ishikawa, "High-speed Ge/Si electro-absorption optical modulator in C-band operation wavelengths," *Opt. Express*, vol. 28, no. 22, pp. 33123–33134, Oct. 2020.

[32] S. Ren, Y. Rong, S. A. Claussen, R. K. Schaevitz, T. I. Kamins, J. S. Harris, and D. A. B. Miller, "Ge/SiGe quantum well waveguide modulator monolithically integrated with SOI waveguides," *IEEE Photon. Technol. Lett.*, vol. 24, no. 6, pp. 461–463, Mar. 2012.

[33] D. Feng, W. Qian, H. Liang, C. -C. Kung, Z. Zhou, Z. Li, J. S. Levy, R. Shafiiha, J. Fong, B. J. Luff, and M. Asghari, "High-speed GeSi electroabsorption modulator on the SOI waveguide platform," *IEEE J. Select. Topics Quantum Electron.*, vol. 19, no. 6, Nov./Dec. 2013, Art. no. 3401710.

[34] S. A. Srinivasan, M. Pantouvaki, S. Gupta, H. T. Chen, P. Verheyen, G. Lepage, G. Roelkens, K. Saraswat, D. Van Thourhout, P. Absil, and J. Van Campenhout, "56 Gb/s germanium waveguide electro-absorption modulator," *J. Lightwave Technol.*, vol. 34, no. 2, pp. 419–424, Jan. 2016.

[35] L. Mastronardi, M. Banakar, A. Z. Khokhar, N. Hattasan, T. Rutirawut, T. Dominguez Bucio, K. M. Grabska, C. Littlejohns, A. Bazin, G. Mashanovich, and F. Y. Gardes, "High-speed Si/GeSi hetero-structure electro absorption modulator," *Opt. Express*, vol. 26, no. 6, pp. 6663–6673, Mar. 2018.

[36] D. Ma, Y. Lin, R. Wen, L. C. Kimerling, and J. Michel, "Strained $Ge_{0.99}Si_{0.01}$ Modulator Arrays for Integrated Broadband Modulation," in *Proc. 2020 IEEE Photon. Conf. (IPC)*, Tul4.4.

[37] S. C. Jain, H. E. Maes, K. Pinardi, and I. De Wolf, "Stresses and strains in lattice-mismatched stripes, quantum wires, quantum dots, and substrates in Si technology," *J. Appl. Phys.*, vol. 79, no. 11, pp. 8145–8165, Jun. 1996.

[38] M. Nishimura, K. Kawashita, and Y. Ishikawa, "Silicon-germanium stressors for germanium photonic devices on silicon," *ECS Trans.*, vol. 86, no.7, pp. 3–10, Jul. 2018.

[39] C. G. Van de Walle, "Band lineups and deformation potentials in the model-solid theory," *Phys. Rev. B.*, vol. 39, no. 3, pp. 1871–1883, Jan. 1989.

[40] Y. P. Varshni, "Temperature dependence of the energy gap in semiconductors," *Physica*, vol. 34, no. 1, pp. 149–154, 1967.

[41] J. Liu, D. D. Cannon, K. Wada, Y. Ishikawa, D. T. Danielson, S. Jongthammanurak, J. Michel, and L. C. Kimerling, "Deformation potential constants of biaxially tensile stressed Ge epitaxial films on Si(100)," *Phys. Rev. B.*, vol. 70, no. 15, Oct. 2004, Art. no. 155309.

[42] F. H. Pollak and M. Cardona, "Piezo-electroreflectance in Ge, GaAs, and Si," *Phys. Rev.*, vol. 172, no. 3, pp. 816–837, Aug. 1968.

[43] L. M. Nguyen, R. Kuroyanagi, T. Tsuchizawa, Y. Ishikawa, K. Yamada, and K. Wada, "Stress tuning of the fundamental absorption edge of pure germanium waveguides," *Opt. Express*, vol. 23, no. 14, pp. 18487–18492, Jul. 2015.

[44] M. V. Fischetti and S. E. Laux, "Band structure, deformation potentials, and carrier mobility in strained Si, Ge, and SiGe alloys," *J. Appl. Phys.*, vol. 80, no. 4, pp. 2234–2252, Aug. 1996.

[45] S. L. Chuang, *Physics of Optoelectronic Devices*, Wiley, New York, 1995, p. 549.

[46] K. Noguchi, M. Nishimura, Y. Tsusaka, J. Matsui, and Y. Ishikawa, “Enhancement of L-band optical absorption in strained epitaxial Ge on Si-on-quartz wafer: Toward extended Ge photodetectors,” *J. Appl. Phys.*, vol. 128, no. 13, Oct. 2020, Art. no. 133107.

[47] Y. Ishikawa and K. Wada, “Germanium for silicon photonics,” *Thin Solid Films*, vol. 518, no. 6, pp. S83–S87, Jan. 2010.

[48] R. Katamawari, K. Kawashita, T. Hizawa, and Y. Ishikawa, “Si-capping-induced surface roughening on the strip structures of Ge selectively grown on an Si substrate,” *J. Vac. Sci. Technol. B*, vol. 39, no. 4, Jul./Aug. 2021, Art. no. 042204.

[49] R. Tsuchiya, R. Oyamada, T. Fukushima, J. A. Piedra-Lorenzana, T. Hizawa, T. Nakai, and Y. Ishikawa, “Low-Loss Hydrogen-Free SiN_x Optical Waveguide Deposited by Reactive Sputtering on a Bulk Si Platform,” *IEEE J. Select. Topics Quantum Electron.*, vol. 28, no. 3, May./Jun. 2022, Art. no. 4400109.

[50] N. Higashitarumizu and Y. Ishikawa, “Enhanced direct-gap light emission from Si-capped n^+-Ge epitaxial layers on Si after post-growth rapid cyclic annealing: impact of non-radiative interface recombination toward Ge/Si double heterostructure lasers,” *Opt. Express*, vol. 25, no. 18, pp. 21286–21300, Sep. 2017.

[51] M. Yako, N. J. Kawai, Y. Mizuno, and K. Wada, “The kinetics of Ge lateral overgrowth on SiO_2”, *MRS Adv.*, vol. 1, no. 23, pp. 1703–1708, Dec. 2015.

[52] A. Gassenq, S. Tardif, K. Guilloy, I. Duchemin, N. Pauc, J. M. Hartmann, D. Rouchon, J. Widiez, Y. M. Niquet, L. Milord, T. Zabel, H. Sigg, J. Faist, A. Chelnokov, F. Rieutord, V. Reboud, and V. Calvo, “Raman-strain relations in highly strained Ge: Uniaxial <100>, <110> and biaxial (001) stress,” *J. Appl. Phys.*, vol. 121, no. 5, Feb. 2017, Art. no. 055702.

[53] H. H. Burke and I. P. Herman, “Temperature dependence of Raman scattering in $Ge_{1-x}Si_x$ alloys,” *Phys. Rev. B.*, vol. 48, no. 20, pp. 15016–15024, Nov. 1993.